Video Article

Semiautomated Longitudinal Microcomputed Tomography-based Quantitative Structural Analysis of a Nude Rat Osteoporosis-related Vertebral Fracture Model

Galina Shapiro[1], Maxim Bez[1], Wafa Tawackoli[2,3,4], Zulma Gazit[1,2,3,5], Dan Gazit[1,2,3,4,5], Gadi Pelled[1,2,3,4]

[1]Skeletal Biotech Laboratory, Hebrew University-Hadassah Faculty of Dental Medicine

[2]Department of Surgery, Cedars-Sinai Medical Center

[3]Board of Governors Regenerative Medicine Institute, Cedars-Sinai Medical Center

[4]Biomedical Imaging Research Institute, Cedars-Sinai Medical Center

[5]Department of Orthopedics, Cedars-Sinai Medical Center

Correspondence to: Gadi Pelled at gadip@ekmd.huji.ac.il

URL: https://www.jove.com/video/55928
DOI: doi:10.3791/55928

Keywords: Bioengineering, Issue 127, Osteoporosis, microcomputed tomography, fracture, nude rat, semiautomated, vertebra

Date Published: 9/28/2017

Citation: Shapiro, G., Bez, M., Tawackoli, W., Gazit, Z., Gazit, D., Pelled, G. Semiautomated Longitudinal Microcomputed Tomography-based Quantitative Structural Analysis of a Nude Rat Osteoporosis-related Vertebral Fracture Model. *J. Vis. Exp.* (127), e55928, doi:10.3791/55928 (2017).

Abstract

Osteoporosis-related vertebral compression fractures (OVCFs) are a common and clinically unmet need with increasing prevalence as the world population ages. Animal OVCF models are essential to the preclinical development of translational tissue engineering strategies. While a number of models currently exist, this protocol describes an optimized method for inducing multiple highly reproducible vertebral defects in a single nude rat. A novel longitudinal semiautomated microcomputed tomography (μCT)-based quantitative structural analysis of the vertebral defects is also detailed. Briefly, rats were imaged at multiple time points post-op. The day 1 scan was reoriented to a standard position, and a standard volume of interest was defined. Subsequent μCT scans of each rat were automatically registered to the day 1 scan so the same volume of interest was then analyzed to assess for new bone formation. This versatile approach can be adapted to a variety of other models where longitudinal imaging-based analysis could benefit from precise 3D semiautomated alignment. Taken together, this protocol describes a readily quantifiable and easily reproducible system for osteoporosis and bone research. The suggested protocol takes 4 months to induce osteoporosis in nude ovariectomized rats and between 2.7 and 4 h to generate, image, and analyze two vertebral defects, depending on tissue size and equipment.

Video Link

The video component of this article can be found at https://www.jove.com/video/55928/

Introduction

More than 200 million people worldwide suffer from osteoporosis[1]. The underlying pathological decrease in bone mineral density (BMD) and altered bone microarchitecture increase bone fragility and, consequently, the relative risk of fracture[2]. Osteoporosis is so prevalent and detrimental to health that the WHO has defined it a major public health concern. Furthermore, as the world's population is expected to age, osteoporosis is expected to become even more common.

Osteoporotic vertebral compression fractures are the most common fragility fractures, estimated at more than 750,000 a year in the US. They are associated with significant morbidity and as much as a nine-times higher mortality rate[3]. In clinical trials, currently available surgical interventions, such as vertebroplasty and kyphoplasty, were found to be no more effective than a sham treatment[4,5], leaving only pain management available to these patients. Since current OVCF treatments are limited, it is imperative to develop an animal model that can replicate the disorder[6,7,8]. Such animal models could facilitate both the investigation of current treatment methods and the development of novel therapies that will translate into clinical practice. Osteoporosis has been induced and sustained in model animals through the administration of a low-calcium diet (LCD) in conjunction with ovariectomy[1,9,10,11,12,13,14,15]. To further model the bone loss associated with OVCFs, vertebral bone defects were established in osteoporotic immunocompetent rats [16,17,18,19,20,21,22,23,24]. In this work, a vertebral defect model of immunocompromised rats with modeled osteoporosis is presented. This novel model can be used to assess cell-based therapies involving stem cells derived from various sources and species for the repair of challenging fractures, such as OVCFs.

Bone imaging is a crucial part of the evaluation of fractures and bone diseases. Advanced imaging methods were developed for the accurate assessment of structural bone changes and regeneration strategies[25]. Among them, μCT imaging has emerged as a non-invasive, easy-to-use, and inexpensive method that provides high-resolution 3D images. μCT imaging has several advantages over other modalities in evaluating osteoporosis patients, as it offers high-resolution 3D bone microarchitecture[26] that can then be quantitatively analyzed. The latter can then be used to compare the therapeutic effects of proposed treatments. Indeed, *in vivo* μCT imaging is a gold standard for vertebral defect regeneration

monitoring[1,16,27]. However, few publications[28,29,30,31] have employed automated registration tools to minimize the user-dependency, interpolation bias, and precision error of µCT imaging-based analysis. Recently, we were the first to use a registration procedure to improve the analysis of bone regeneration in a standardized bone void, as explained in this protocol[32] .

The method described here can be used to study the effect of novel cell therapies for OVCFs, unhindered by host T-cell responses that might reject xenogeneic or allogeneic cells. Osteoporosis is induced in young rats through ovariectomy (OVX) and 4 months of an LCD. The young age of the OVX rats, combined with the LCD allowed, us to reach a low peak bone mass, mimicking postmenopausal osteoporosis by leading to irreversible bone loss. This can be explained partly by the fact that, during the LCD and at around 3 months of age, the rats transition from the bone modeling to remodeling phase at the lumbar vertebrae[33], thereby increasing the likelihood of maintaining the osteoporosis over time. Using young animals makes this model more cost effective, as they cost less. Nonetheless, it is limited by inherently not accounting for the biological changes in the aging animal.

Protocol

All animal experiments were performed under a protocol approved by the Institutional Animal Care and Use Committee (IACUC) of Cedars-Sinai Medical Center (Protocol # 3609). Anesthesia was administered for all imaging and surgical procedures. All animals were housed in accordance with approved IACUC protocols.

NOTE: The experimental design of this protocol is shown in **Figure 1**. Purchase six-week-old rats with their ovaries surgically removed and feed them an LCD consisting of 0.01% calcium and 0.77% phosphate. After a period of 4 months of an LCD, drill a critical-size vertebral defect in the fourth and fifth lumbar vertebral bodies (L4-L5). Following surgery, image the rats on day 1 and weeks 2, 4, 8, and 12 after defect establishment. Locate defect margins on the day 1 scan, reorient to a standard position, and define a cylindrical volume of interest (VOI). Automatically register the subsequent µCT scans (*i.e.*, for weeks 2, 4, 8, and 12) of each rat to the standard position defined for the corresponding day 1 scan. Apply the day 1 predefined VOI to the registered scans. Assess the bone volume density and apparent density of the VOIs.

1. Induction of Osteoporosis

1. Put six-week-old athymic ovariectomized rats on 4 months of an LCD consisting of 0.01% calcium and 0.77% phosphate.
2. Switch back to a normal diet.
   NOTE: These rats will be referred to as "osteoporotic rats" hereafter.

2. Vertebral Defect Model

NOTE: The timing is 40 - 50 min per animal.

1. Autoclave all surgical tools prior to surgery.
2. **In the case of multiple surgeries, sterilize all surgical tools.**
   1. Wash the tools and place them in a sonicator bath for 5 min. Place them in a hot bead sterilizer set to 250 °C for 20 s. Allow the tools to cool down for 5 min.
3. **Induce anesthesia.**
   1. Place the osteoporotic rat in the induction chamber attached to an anesthesia machine with a central scavenging system. Induce anesthesia using 5% isoflurane in 100% oxygen and maintain via nose cone at 2 - 3% isoflurane. Use vet ointment on the eyes to prevent dryness while under anesthesia.
   2. Apply a toe-pinch stimulus to ensure adequate plane of anesthesia. If no response is noted, initiate the procedure.
4. Place the anesthetized rat in dorsal recumbency on a heating pad (37 °C) and stretch the limbs using a magnetic fixator retraction system (**Figure 2A**).
   NOTE: The temperature of the heating pad is important for the prevention of hypothermia, since an anesthetized rat is unable to regulate its body temperature.
5. Shave the abdominal area using an electric shaver. Swab it with iodine-based antiseptic and chlorhexidine gluconate 0.5% followed by 70% ethanol.
6. Inject the rat with carprofen (5 mg/kg bodyweight (BW), subcutaneous (SQ)) before beginning the surgical procedure.
7. Use a sterile scalpel to cut the skin. Begin the incision 1 cm below the xiphoid process and cut through the midline (~5 - 8 cm) (**Figure 2B**).
8. Use surgical scissors to make an incision of the aponeurosis through the linea alba to access the abdominal cavity (**Figure 2C**).
9. Expose the abdominal cavity using retractors (**Figure 2D**).
10. Deflect the intestines to the right of the rat to expose the abdominal aorta and the left kidney (**Figure 2E**). Palpate the lumbar spine before proceeding to expose it. To avoid dehydration, use sterile soaked gauzes with sterile saline solution to wrap the internal organs.
11. Use thermocautery to expose in layers the anterior aspect of lumbar vertebral bodies L4-5 and isolate them from the surrounding connective tissue and muscles (**Figure 2F-G**).
    NOTE: Thermocautery should be used to control bleeding during the dissection.
12. Use a sterile cotton swab saturated with sterile saline to remove blood and residual tissue from the L4 vertebrae. Use a sterile Trephine drill bur (~2 mm in diameter) to drill a 5 mm-deep bone defect in the center of the exposed anterior aspect of the vertebral body **(Figure 2H-I).**
    NOTE: Apply minimal pressure to drill through only the ventral cortex and underlying trabecular bone; avoid drilling through the dorsal cortex. Note that the vertebrae of osteoporotic rats are very fragile. Use a cotton swab to clean the defect and apply pressure to stop bleeding, if present.
13. Repeat step 2.11 on the L5 vertebra to create a total of 2 defects per rat (**Figure 2J**).
14. Return the intestines to the abdominal cavity.

15. Use a vicryl synthetic absorbable surgical suture (3-0 vicryl undyed 27" SH taper) in a continuous pattern to suture the aponeurosis (**Figure 2K**).
16. Close the skin using a 4-0 monofilament nylon non-absorbable suture in a simple interrupted pattern (**Figure 2L**).
17. Apply 100 µL of topical skin adhesive on top of the skin sutures and between them to ensure the complete closure of the skin.
18. Inject the rat with warm (37 °C) lactated ringer's solution (1CC/100 g BW, SQ) to prevent hypothermia and dehydration.
19. Inject the rat with buprenorphine (0.5 mg/kg BW, SQ) prior to the surgery and every 8 - 12 h for post-op pain relief as needed.
20. Do not leave the animal unattended until it has regained sufficient consciousness to maintain sternal recumbency. Also, do not return an animal that has undergone surgery to the company of other animals until it has fully recovered.
21. After the animal has recovered on the heating pad, return it to its cage.
    NOTE: House the rats individually (*i.e.,* in separate cages) to prevent rat-to-rat mutilation of the sutures and wound.
22. Place chow soaked in water in a Petri dish on the cage floor for a few days post-op to help the rats reach the food.
23. Administer carprofen (5 mg/kg BW, SQ) 24 h post-surgery for pain relief every 24 h as needed.
24. Remove the skin sutures while the animal is under 2% isoflurane anesthesia 10 - 14 days post-operation.

3. MicroCT Scanning

NOTE: The timing is 30 - 40 min per animal.

1. On the day following the surgical procedure, place the osteoporotic rat in the induction chamber attached to an anesthesia machine with a central scavenging system. Induce anesthesia using 5% isoflurane in 100% oxygen and maintain via nose cone at 2 - 3% isoflurane.
2. Scan the rat using an *in vivo* µCT scanner. Repeat scanning for the longitudinal analysis of bone regeneration.
   NOTE: Make sure that all animals are scanned using the same settings (*i.e.,* X-ray energy, scanning medium, intensity, voxel size, and image resolution) and in a similar orientation. For example: X-ray energy, 55 kVP; current, 145 µA; voxel size, 35 µm; increments, 115 µm; and integration time, 200 ms; with the samples in PBS. Refer to Bouxtein *et al.*[34] for further explanations and considerations involved in rodent µCT scanning for an assessment of bone microstructure. Ideally, the highest scan resolution available would be used for all scans; however, higher-resolution scans require longer acquisition times, generate large data sets, and expose the animals to more ionizing radiation. The latter may introduce unwanted effects, including decreased fracture healing.Therefore, the tradeoff between additional data and scan time should be carefully considered.

4. Vertebral Separation

NOTE: The timing is 20 - 30 min per sample.

1. **Contour the vertebra of interest, as demonstrated in Figure 3A-I. Make sure to include all parts of the vertebra while excluding parts that belong to adjacent vertebrae.**
   1. Click on "µCT evaluation program" and select the sample from the menu.
   2. Contour each slice using the mouse.
   3. Use the "Z" bar to go to the next slice.
2. Save the contoured vertebra as a separate file (**Figure 3J-K**) by clicking on "File" → "Save GOBJ" every couple of slices.

5. Definition of the VOI for Longitudinal Quantitative Evaluation

NOTE: The following steps depend on whether the scan is from day 1 after surgery (reference vertebra) or from the subsequent time points (target vertebrae).

1. **Reference vertebra.**
   NOTE: The timing is 20 - 30 min per sample.
   1. For Z-rotation, measure the angle of the margins using an XY-slice from the center of the defect (**Figure 4A-B**).
      1. On the Z-plane, go to the area of the vertebra where the defect is most clear and screen capture the vertebra.
      2. In a presentation software, prepare a rectangle-shaped object that will fit into the defect.
      3. Rotate the image of the vertebra such that the defect faces upwards and the defect margins are parallel to the sides of the rectangle.
      4. Measure the angle of rotation (right-click on the image → "Format Picture" → "Size").
      5. Use the measured angle to rotate the vertebra (**Figure 4C**).
         1. Open a new DECterm window ("Session manager" → "Applications" → "DECterm").
         2. Run "ipl":
         3. Ipl> **turn3d**
         4. -input [in]>
         5. -output [out]>
         6. -turnaxis_angles [0.000 90.000 90.000]> 90 90 0
         7. -turnangle [0.000]> measured angle
         8. -img_interpol_option [1]>
   2. For X-rotation, measure the angle of the margins using a YZ-slice from the center of the defect (**Figure 4D-E**). Use the measured angle to rotate the vertebra (**Figure 4F**).
      1. Click on "YZ" in "uCT evaluation program" and repeat steps 5.1.1.1-5.1.1.5.2.
      2. Ipl> **isq**

3. -aim_name [in]>
4. -isq_filename [default_file_name]> Insert the ISQ file directory (*e.g.*, "DK0: [MICROCT.DATA.GAZIT.MAXIM.80.DAY1]Z2102970.ISQ")
5. -pos [0 0 0]>
6. -dim [-1 -1 -1]>

3. Flip the rotated vertebra by changing the XY-plane to the ZX-plane.
    1. Open a new DECterm window ("Session manager" → "Applications" → "DECterm").
    2. Run "ipl":
    3. Ipl> **flip**
    4. -input [in] > out
    5. -input [out] > out2
    6. -new_xydir [yz] > zx

4. Define the VOI.
    1. Draw a circular contour of the defect using a slice from the center of the defect by selecting the circular contour icon in "uCT evaluation program" (**Figure 6A**). Copy that contour and paste it on all slices in the defect (**Figure 6B**).
    NOTE: Since all defects were created using the same procedure, analyze the same number of slices and, subsequently, the total volume (TV) for all samples.

2. **Target vertebra.**
NOTE: The timing is 10 - 20 min per sample.
    1. Load the DICOM files of both the target and the reference vertebrae to the main window of the image analysis software.
    NOTE: To avoid grayscale value changes, define the same output data type as the original DICOM files in the load menu.
    2. Register to the reference vertebra.
        1. Launch the "3-D Voxel Registration" module and input the reference vertebra as the "Base Volume" and the target vertebra as the "Match Volume." Click "Register" to register the vertebrae (**Figure 5**).

    3. Save the registered file using the same data type and import it to a µCT environment.
    4. Apply the VOI.
        1. Apply the VOI defined for the reference vertebra to the registered target vertebra by clicking "uCT evaluation program" → "File" → "Load GOBJ" and selecting the GOBJ previously created. Check that the VOI and defect are concentric.

6. MicroCT Analysis

NOTE: The timing is 10 - 20 min per sample.

1. Send the VOI for evaluation using a µCT evaluation program (**Figure 6**).
NOTE: Make sure to use the same parameters when analyzing all VOIs. Make sure the threshold is set high enough to omit background noise with minimal loss of bone. If a radiopaque biomaterial is used, a number of strategies could be used to analyze bone formation. If there is a difference in density between the biomaterial and bone tissue, the biomaterial could be segmented out[35,36]. Otherwise, the investigators could qualitatively evaluate the differences in bone formation between experimental groups.

7. Euthanasia

1. PPlace the osteoporotic rat in the induction chamber attached to an anesthesia machine. Induce anesthesia using 5% isoflurane in 100% oxygen.
2. Maintain anesthesia via nose cone and perform euthanasia by incising the chest cavity to produce a bilateral pneumothorax[37].

Representative Results

Using this protocol, one can image and quantify the regeneration of n = 8 modeled osteoporotic vertebral defects across different time points. The anatomic match obtained by the registration procedure allows for the analysis of the same VOI at all time points. This results in a highly accurate longitudinal 3D histomorphometric analysis, even when the margins of the original defect are no longer recognizable. We used five time points (day 1, week 2, week 4, week 8, and week 12) as an example for the longitudinal evaluation of bone regeneration (**Figure 7**). Regeneration can be evaluated both by the qualitative assessment of 2D cross-sections and 3D images (as illustrated in **Figure 7A**) and by the quantitative comparison of the bone quantity (BVD) and quality (AD) (**Figure 7B**). The following morphometric indices can be determined for newly formed bone: (i) TV, including bone and soft-tissue volumes (TV, mm^3); (ii) volume of mineralized tissue (BV, mm^3); (iii) bone volume density (BV/TV); and (iv) bone mineral density (BMD, mg hydroxyapatite per cm^3). Specifically, minimal bone formation (5% increase in bone volume density) was observed 2 weeks after defect establishment. After two weeks, no significant differences in bone formation were observed when compared to later time points. Overall, although there was some degree of bone formation, which peaked at approximately 10% by Week 8, it was minimal enough to maintain the bone void over time.

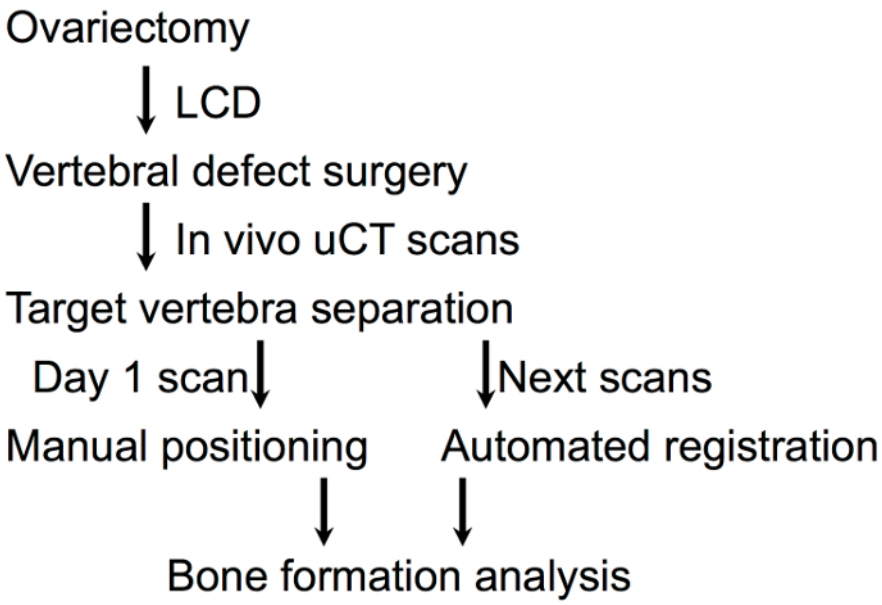

Figure 1: Protocol Design. The key steps in the protocol are outlined. First, ovariectomized nude rats subjected to four months of a low calcium diet (LCD) were operated upon to create standard critical-sized defects in two lumbar vertebral bodies. The rats were imaged on day 1 and weeks 2, 4, 8, and 12 post-op. The day 1 scan was reoriented to a standard position, and a cylindrical VOI was defined using the defect margins. Subsequent μCT scans of each rat were automatically registered to the standard position defined for the corresponding day 1 scan. The day 1 predefined VOI was then applied to the registered scans. The bone volume density and apparent density of the VOI were used to assess new bone formation. Please click here to view a larger version of this figure.

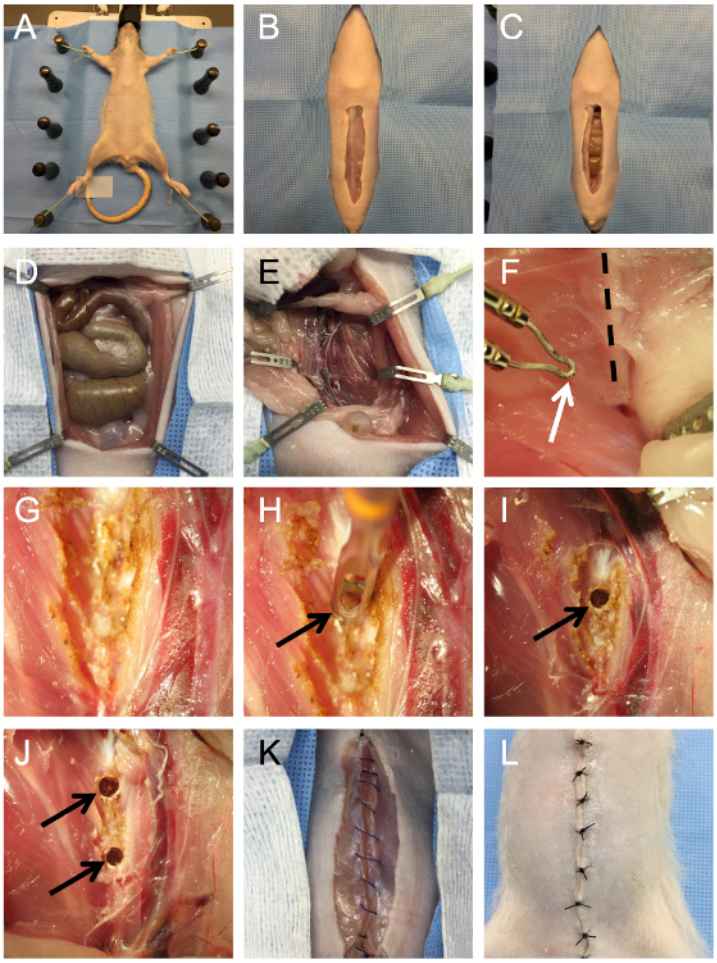

Figure 2: Vertebral Defect Surgery. The key steps in the surgical generation of vertebral defects are illustrated. First, rats were placed on a heating pad (**A**). A midline incision was made through the skin (**B**) and then the linea alba (**C**) to expose the abdominal cavity (**D**). The intestines were reflected to expose the posterior abdominal wall (**E**), and the lumbar spine was exposed using thermocautery (arrow, **F-G**). Defects were drilled in the fourth (**H**, arrow pointing to the drill; **I**, arrow pointing to the defect) and fifth (**J**, arrows pointing to defects) lumbar vertebral bodies. Finally, the aponeurosis (**K**) and skin (**L**) were sutured. Please click here to view a larger version of this figure.

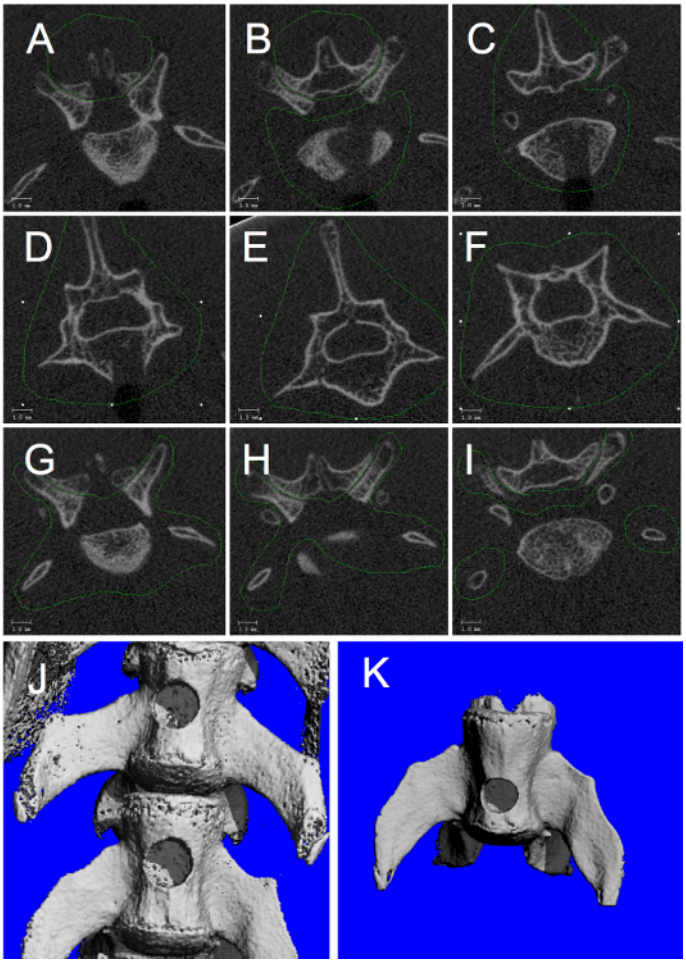

Figure 3: Vertebra Separation. The key steps in the contouring of a vertebra of interest are shown. (**A-I**) Contoured (green line) representative 2D slices along the length axis of a vertebra are shown. A 3D representation of the full spine (**J**) can be compared to the separated vertebra (**K**). Please click here to view a larger version of this figure.

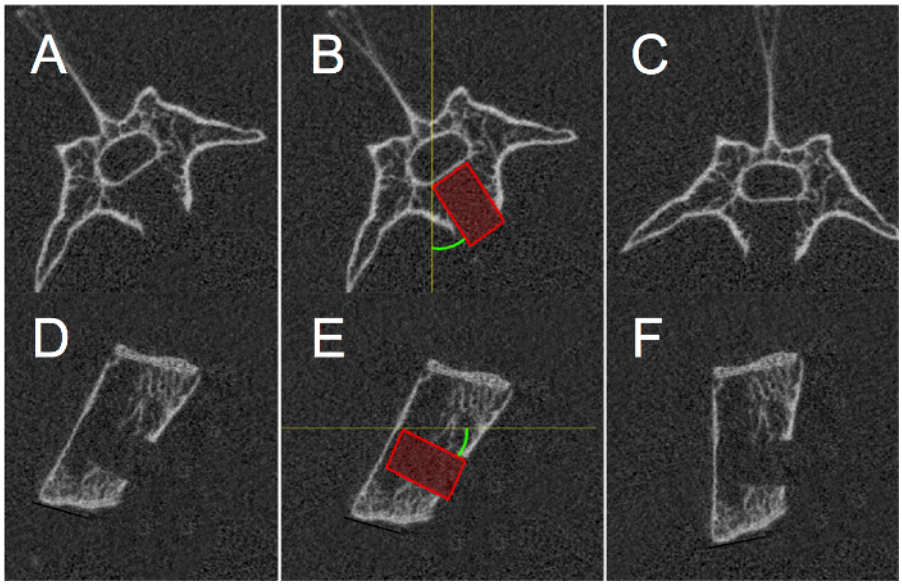

Figure 4: Reference Vertebra Positioning. Representative slices in two planes are shown of a vertebra before and after rotation to a standard position. First, using a representative XY-slice (**A**), the angle (**B**, green) needed to rotate the defect (**B**, red square) to become parallel to the Y-axis (**B**, yellow) is determined and then used to create the rotated image (**C**). Then, using a representative YZ-slice (**D**), the angle (**E**, green) needed to rotate the defect (**E**, red square) to become parallel to the Z-axis (**E**, yellow) is determined and then used to create the rotated image (**F**). Please click here to view a larger version of this figure.

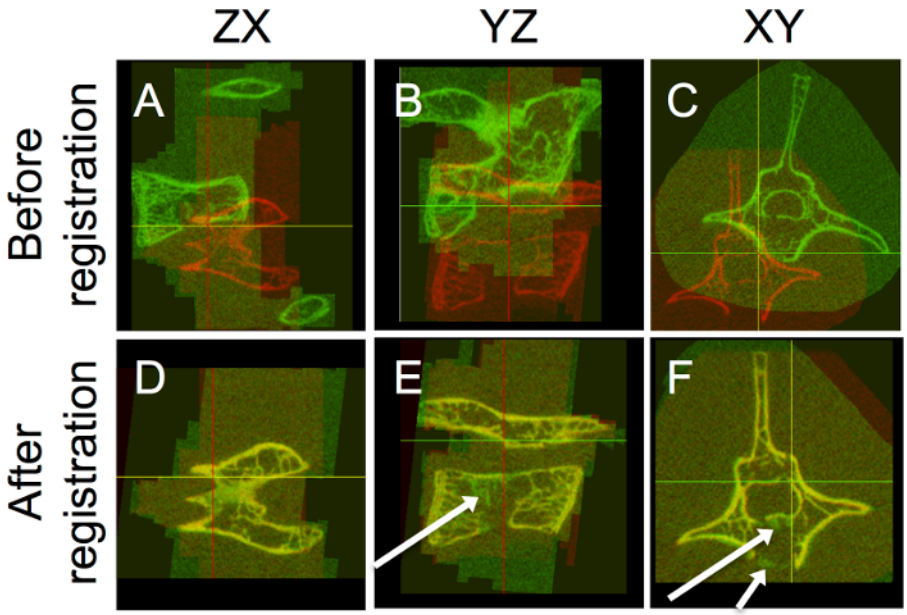

Figure 5: Target Vertebra Registration. Representative slices at three planes of the target vertebra (marked in green) and reference vertebra (marked in red) before (**A-C**) and after (**D-E**) registration are shown. Note the yellow color, indicating overlap between target and reference vertebrae, and the white arrows that point to green bone after regeneration, indicating bone formation. Please click here to view a larger version of this figure.

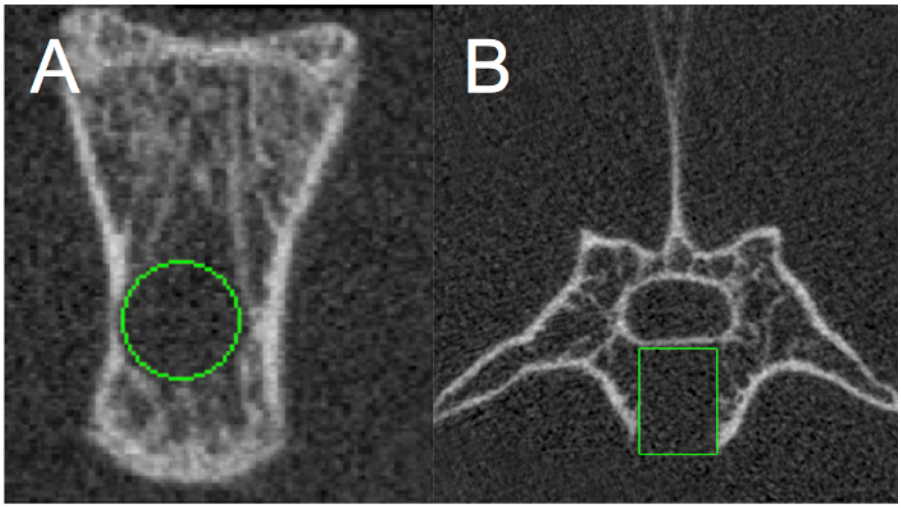

Figure 6: VOI Analysis. Representative slices in two planes with the contoured volume of interest are shown. A circular contour is positioned at the center of the defect in a representative ZX-slice (**A**). After contouring all ZX-slices, the complete defect volume can be seen in the XY-plane (**B**). Please click here to view a larger version of this figure.

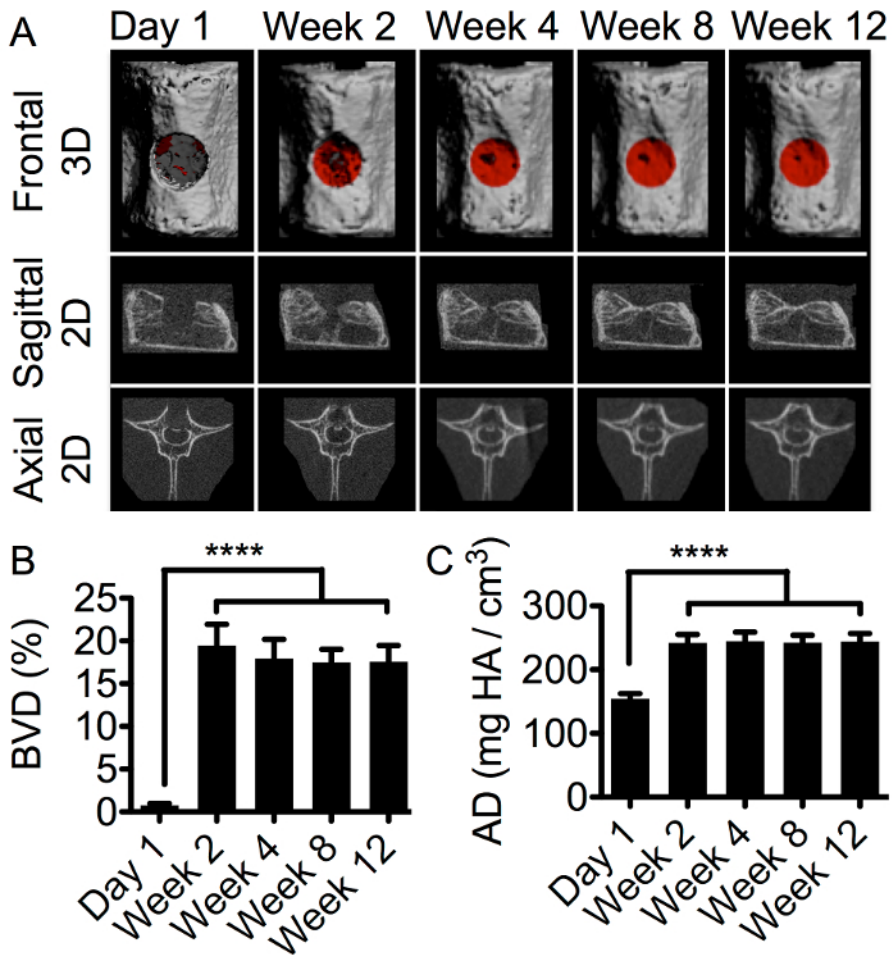

Figure 7: Longitudinal Analysis of Vertebral Defect Regeneration. Qualitative and quantitative representative bone regeneration analysis results are shown. (**A**) A representative vertebral defect at various time points is depicted in each panel as a frontal 3D image (top panel) with bone formation in the void indicated in red, a sagittal 2D image (middle panel), and an axial 2D image (bottom panel). The quantitative analysis of bone formation in the voids was performed. Bone volume density (**B**) and apparent density (**C**) were calculated and compared using a repeated measures two-way ANOVA with Bonferroni correction for multiple comparisons. The error bars represent SEM. **** - p<0.0001. Please click here to view a larger version of this figure.

Steps	Problem	Possible reason	Solution
2.3	Animal gasping under anesthesia	Excess isoflurane delivery	Reduce the concentration of isoflurane delivered to the animal.
	Animal responds to toe pinch	Insufficient isoflurane delivery	Increase the concentration of isoflurane.
2.7-2.12	Heavy bleeding	Vascular damage	Use a sterile cotton swab to apply pressure or cautery to stop bleeding.
	The animal has difficulty breathing	The diaphragm was punctured	Euthanize the animal to prevent suffocation.
	Leakage of intestinal contents	The gastrointestinal tract was punctured	Euthanize the animal to prevent further complications. Prevent it by lifting the aponeurosis away from underlying intestines before cutting.
	Blood emerges from the drilling site	A blood vessel was punctured	Apply a sterile cotton swab until bleeding stops.
	Animal suddenly shakes during drilling	The drill went too deep and damaged the spinal cord	Euthanize the animal to prevent further complications.
	The bone defect looks incomplete	The drill didn't go deep enough	Reposition the drill head inside the defect and drill deeper
2.15-2.24	Suture breaks	The suture was pulled too tightly	Replace the entire suture. If breaking occurs often, use a size thicker suture.
	Animal is slow to recover from anesthesia	The animal is hypothermic	Increase the temperature of the heating pad or apply an additional source of heating (e.g. heating lamp).
	Sutures are open	The sutures were placed loosely, or the animal did strenuous activity	Reapply the sutures and apply Dermabond directly to the sutures and between them.
3	Scanned image appears with low resolution, noisy or scattered	Scanning parameters need to be adjusted	Adjust the parameters of the scanning protocol. Refer to Bouxsein et al. for more guidelines for scanning.
	Scanned image appears blurry	The animal moved during the scanning process	Rescan the animal. If movement continues, increase isoflurane concentration.
5	The registration of target vertebra wasn't successful	Vertebral separation wasn't done properly	Recontour the vertebra: Make sure all parts of vertebra are included, and exclude any adjacent structures.
		Large difference in positioning of vertebrae	Reposition the target vertebra into the same orientation as the reference vertebra using rotations and flip (Step 29A).
		Analyze can't properly recognize the bone structures	Apply a threshold in the registration module to remove the background noise from bone samples.
		The registered vertebrae are different	Create 3d images of your samples and match the correct vertebrae across the different time points.
6	The total volume (TV) is different between samples	Either a different numbers of slices or a different contour was used	Make sure to always use the same contour size and the same number of slices.
	Bone mineral density (BMD) value is abnormal	Inadequate calibration of microCT	Calibrate the microCT for correct hydroxyapatite standards

Table 1: Troubleshooting. Potential problems and solutions are presented for different steps in the protocol.

Discussion

Osteoporosis is the most prevalent cause of vertebral compression fractures caused by an increased load on the spine and that result in the collapse of the vertebral body. However, it is practically impossible to generate an injury in a rodent that authentically replicates a similar vertebral collapse. Instead, researchers create a cylindrical void in the center of the vertebral body to mimic OVCFs[16,17,18,19,20,21,24,38,39]. Since there is no consistency in the literature in terms of defect size, a critical-sized defect was defined as one that does not spontaneously heal fully without an intervention within 3 months post-op[16,17].

Although the method of combining ovariectomy with an LCD to rapidly induce osteoporosis was previously published[1,13], we were the first to show that applying this approach to athymic rats results in an efficient, rapid, and irreversible decrease in vertebral trabecular bone volume and mineral density[40]. This is a reproducible small-animal model that is unhindered by the rodent immune system and that does not have a need for added immunosuppression, as used by others[24].

Our surgical protocol generated multiple identical critical lumbar vertebral defects[40]. This results in highly consistent and easily comparable and quantifiable defects across animals. We believe that defects produced using this approach are superior to vertebral defect models generated in caudal vertebrae[1,19,41] because the rat tail is subjected to biomechanical forces that are significantly different from those involving the rat lumbar spine.

Critical steps within this protocol include avoiding intra-operative hypothermia and taking caution when drilling the fragile vertebrae of ovariectomized nude rats after an LCD. After generating the vertebral defect, it is monitored via a temporal sequence of *in vivo* µCT scans at set time points for the longitudinal assessment of bone repair. Maintaining the same scan settings is critical. The vertebrae are then contoured and separated from the rest of the scan. Contouring an identical total volume for all scans of a vertebra and avoiding grayscale value changes are critical. A commercially available multiple image registration algorithm facilitates the extraction of anatomically corresponding baseline VOIs to all subsequent time points. Finally, these VOIs are analyzed for bone volume, apparent density, *etc*. It is critical to analyze all VOIs using the same parameters. This technique provides a highly accurate and straightforward longitudinal 3D µCT analysis that is not user-dependent.

This method could be applied to any longitudinal bone defect regeneration analysis. The vertebral defect model used here is a convenient model for this application, as its bone structure is unique and can be easily registered to the same anatomical position. However, any bone regeneration could be analyzed under the same conditions by properly separating the same bone of interest throughout the longitudinal scans. It is imperative to include separated bone samples with the same anatomical features. This potential problem and others are described in **Table 1**, along with possible reasons and suggested solutions. The anatomic match obtained by the registration procedure can only occur if the samples include the same anatomical features. The registration will allow the user to apply the exact predefined VOI of the first scan to all remaining time points, resulting in a highly accurate 3D histomorphometric analysis over time. Bone volume density and apparent density of the VOI can be used to assess new bone formation.

While potentially widely applicable, the model presented here is not without limitations. The use of athymic nude rats could be considered a limitation, as it could potentially mask some immune-mediated processes that may be of importance to regeneration. Second, modeling osteoporosis through a combination of ovariectomy and an LCD in young rats, as previously published[1,13], is limited in its ability to mimic the biology of the elderly patient population. Third, OVCFs were modeled by a surgical procedure, as the only other animals to have osteoporosis-related fractures are primates[42]. Finally, while the rat lumbar spine is the best available model for the human lumbar spine—where most vertebral fractures develop—the lack of axial weight bearing in the rodent spine is also a limitation.

This protocol is modular and therefore could be easily modified to the researcher's needs. For example, the athymic ovariectomized rats could be used to study other osteoporosis-related fractures. Should a researcher choose to use our approach to semiautomated bone regeneration analysis, it could be applied to any fracture model using longitudinal structural imaging, not necessarily micro-computed tomography. Furthermore, additional information could be gathered by simultaneously using additional imaging modalities such as magnetic resonance imaging.

The OVCF model presented in this protocol could be used to study novel therapeutic approaches to this clinically unmet need. Furthermore, our semiautomated analysis approach can be successfully used to perform a similar analysis that is less user-dependent and provides better accuracy than other methods[16]. Particularly noteworthy is the fact that we used commercially available visualization and analysis software that can be used by any researcher—software that supports additional imaging modalities, such as magnetic resonance imaging and nuclear imaging. Therefore, we believe that this method is highly generalizable and is only limited by the availability of *in vivo* imaging capabilities and registration software.

Disclosures

This research was supported by a grant from the California Institute for Regenerative Medicine (CIRM) (TR2-01780).

Acknowledgements

The research was supported by a grant from the California Institute for Regenerative Medicine (CIRM) (TR2-01780).

References

1. Wang, M. L., Massie, J., Perry, A., Garfin, S. R., Kim, C. W. A rat osteoporotic spine model for the evaluation of bioresorbable bone cements. *Spine J.* **7** (4), 466-474 (2007).
2. Consensus development conference: prophylaxis and treatment of osteoporosis. *Am J Med.* **90** (1), 107-110 (1991).
3. Center, J. R., Nguyen, T. V., Schneider, D., Sambrook, P. N., Eisman, J. A. Mortality after all major types of osteoporotic fracture in men and women: an observational study. *Lancet.* **353** (9156), 878-882 (1999).
4. Buchbinder, R. *et al.* A randomized trial of vertebroplasty for painful osteoporotic vertebral fractures. *N Engl J Med.* **361** (6), 557-568 (2009).
5. Kallmes, D. F. *et al.* A randomized trial of vertebroplasty for osteoporotic spinal fractures. *N Engl J Med.* **361** (6), 569-579 (2009).
6. Kado, D. M. *et al.* Vertebral fractures and mortality in older women: a prospective study. Study of Osteoporotic Fractures Research Group. *Arch Intern Med.* **159** (11), 1215-1220 (1999).
7. Silverman, S. L. The clinical consequences of vertebral compression fracture. *Bone.* **13** (Suppl 2), S27-31 (1992).
8. Ross, P. D. Clinical consequences of vertebral fractures. *Am J Med.* **103** (2A), 30S-43S (1997).
9. Saito, T., Kin, Y., Koshino, T. Osteogenic response of hydroxyapatite cement implanted into the femur of rats with experimentally induced osteoporosis. *Biomaterials.* **23** (13), 2711-2716 (2002).
10. Koshihara, M., Masuyama, R., Uehara, M., Suzuki, K. Effect of dietary calcium: Phosphorus ratio on bone mineralization and intestinal calcium absorption in ovariectomized rats. *Biofactors.* **22** (1-4), 39-42 (2004).
11. Martin-Monge, E. *et al.* Validation of an osteoporotic animal model for dental implant analyses: an in vivo densitometric study in rabbits. *Int J Oral Maxillofac Implants.* **26** (4), 725-730 (2011).
12. Agata, U. *et al.* The effect of different amounts of calcium intake on bone metabolism and arterial calcification in ovariectomized rats. *J Nutr Sci Vitaminol (Tokyo).* **59** (1), 29-36 (2013).
13. Govindarajan, P. *et al.* Bone matrix, cellularity, and structural changes in a rat model with high-turnover osteoporosis induced by combined ovariectomy and a multiple-deficient diet. *Am J Pathol.* **184** (3), 765-777 (2014).
14. Govindarajan, P. *et al.* Implications of combined ovariectomy/multi-deficiency diet on rat bone with age-related variation in bone parameters and bone loss at multiple skeletal sites by DEXA. *Med Sci Monit Basic Res.* **19**, 76-86 (2013).
15. Alt, V. *et al.* A new metaphyseal bone defect model in osteoporotic rats to study biomaterials for the enhancement of bone healing in osteoporotic fractures. *Acta Biomater.* **9** (6), 7035-7042 (2013).
16. Liang, H. *et al.* Use of a bioactive scaffold for the repair of bone defects in a novel reproducible vertebral body defect model. *Bone.* **47** (2), 197-204 (2010).
17. Liang, H., Li, X., Shimer, A. L., Balian, G., Shen, F. H. A novel strategy of spine defect repair with a degradable bioactive scaffold preloaded with adipose-derived stromal cells. *Spine J.* **14** (3), 445-454 (2014).
18. Fujishiro, T. *et al.* Histological evaluation of an impacted bone graft substitute composed of a combination of mineralized and demineralized allograft in a sheep vertebral bone defect. *J Biomed Mater Res A.* **82** (3), 538-544 (2007).
19. Sheyn, D. *et al.* Gene-modified adult stem cells regenerate vertebral bone defect in a rat model. *Mol Pharm.* **8** (5), 1592-1601 (2011).
20. Phillips, F. M. *et al.* In vivo BMP-7 (OP-1) enhancement of osteoporotic vertebral bodies in an ovine model. *Spine J.* **6** (5), 500-506 (2006).
21. Kobayashi, H. *et al.* Long-term evaluation of a calcium phosphate bone cement with carboxymethyl cellulose in a vertebral defect model. *J Biomed Mater Res A.* **88** (4), 880-888 (2009).
22. Turner, T. M. *et al.* Vertebroplasty comparing injectable calcium phosphate cement compared with polymethylmethacrylate in a unique canine vertebral body large defect model. *Spine J.* **8** (3), 482-487 (2008).
23. Zhu, X. S. *et al.* A novel sheep vertebral bone defect model for injectable bioactive vertebral augmentation materials. *J Mater Sci Mater Med.* **22** (1), 159-164 (2011).
24. Vanecek, V. *et al.* The combination of mesenchymal stem cells and a bone scaffold in the treatment of vertebral body defects. *Eur Spine J.* **22** (12), 2777-2786 (2013).
25. Geusens, P. *et al.* High-resolution in vivo imaging of bone and joints: a window to microarchitecture. *Nat Rev Rheumatol.* **10** (5), 304-313 (2014).
26. Genant, H. K., Engelke, K., & Prevrhal, S. Advanced CT bone imaging in osteoporosis. *Rheumatology (Oxford).* **47** (Suppl 4), 9-16, iv9-16 (2008).
27. Kallai, I. *et al.* Microcomputed tomography-based structural analysis of various bone tissue regeneration models. *Nature Protocols.* **6** (1), 105-110 (2011).
28. Lambers, F. M., Kuhn, G., Schulte, F. A., Koch, K., Muller, R. Longitudinal assessment of in vivo bone dynamics in a mouse tail model of postmenopausal osteoporosis. *Calcif Tissue Int.* **90** (2), 108-119 (2012).
29. de Bakker, C. M. *et al.* muCT-based, in vivo dynamic bone histomorphometry allows 3D evaluation of the early responses of bone resorption and formation to PTH and alendronate combination therapy. *Bone.* **73**, 198-207 (2015).
30. Lan, S. H. *et al.* 3D image registration is critical to ensure accurate detection of longitudinal changes in trabecular bone density, microstructure, and stiffness measurements in rat tibiae by in vivo microcomputed tomography (mu CT). *Bone.* **56** (1), 83-90 (2013).
31. Nishiyama, K. K., Campbell, G. M., Klinck, R. J., Boyd, S. K. Reproducibility of bone micro-architecture measurements in rodents by in vivo micro-computed tomography is maximized with three-dimensional image registration. *Bone.* **46** (1), 155-161 (2010).
32. Sheyn, D. *et al.* PTH Induces Systemically Administered Mesenchymal Stem Cells to Migrate to and Regenerate Spine Injuries. *Mol Ther.* **24** (2), 318-330 (2016).
33. Lelovas, P. P., Xanthos, T. T., Thoma, S. E., Lyritis, G. P., Dontas, I. A. The laboratory rat as an animal model for osteoporosis research. *Comp Med.* **58** (5), 424-430 (2008).
34. Bouxsein, M. L. *et al.* Guidelines for assessment of bone microstructure in rodents using micro-computed tomography. *J Bone Miner Res.* **25** (7), 1468-1486 (2010).
35. de Lange, G. L. *et al.* A histomorphometric and micro-computed tomography study of bone regeneration in the maxillary sinus comparing biphasic calcium phosphate and deproteinized cancellous bovine bone in a human split-mouth model. *Oral Surg Oral Med Oral Pathol Oral Radiol.* **117** (1), 8-22 (2014).

36. Ramalingam, S. *et al.* Guided bone regeneration in standardized calvarial defects using beta-tricalcium phosphate and collagen membrane: a real-time in vivo micro-computed tomographic experiment in rats. *Odontology.* **104** (2), 199-210 (2016).
37. Leary, S. *et al. AVMA guidelines for the euthanasia of animals: 2013 edition.* (2013).
38. Wang, M. L., Massie, J., Allen, R. T., Lee, Y. P., Kim, C. W. Altered bioreactivity and limited osteoconductivity of calcium sulfate-based bone cements in the osteoporotic rat spine. *Spine J.* **8** (2), 340-350 (2008).
39. Liang, H., Li, X., Shimer, A. L., Balian, G., Shen, F. H. A novel strategy of spine defect repair with a degradable bioactive scaffold preloaded with adipose-derived stromal cells. *Spine J.* **14** (3), 445-454 (2013).
40. Sheyn, D. *et al.* PTH induces systemically administered mesenchymal stem cells to migrate to and regenerate spine injuries. *Mol Ther.* **24** (2), 318-330 (2015).
41. Matthieu, R. *et al.* A new rat model for translational research in bone regeneration. *Tissue Eng Part C Methods.* (2015).
42. Turner, A. S. Animal models of osteoporosis--necessity and limitations. *Eur Cell Mater.* **1**, 66-81 (2001).

